Chinese Chemical Letters 32 (2021) 3575–3578

Contents lists available at ScienceDirect

Chinese Chemical Letters

journal homepage: www.elsevier.com/locate/cclet

Communication

# Fast self-assembled microfibrillated cellulose@MXene film with high-performance energy storage and superior mechanical strength

Zhirong Zhang, Zhongping Yao*, Zhaohua Jiang

*School of Chemistry and Chemical Engineering, State Key Laboratory of Urban Water Resource and Environment, Harbin Institute of Technology, Harbin 150001, China*

ARTICLE INFO

*Article history:*
Received 17 February 2021
Received in revised form 9 March 2021
Accepted 10 March 2021
Available online 17 March 2021

*Keywords:*
MXene
Microfibrillated cellulose
Supercapacitor
Self-assemble
Microgel

ABSTRACT

The trade-off between the electrochemical performance and mechanical strength is still a challenge for $Ti_3C_2T_x$ free-standing electrode. Herein, a facile approach was proposed to fabricate a Microfibrillated cellulose@$Ti_3C_2T_x$ (MFC@$Ti_3C_2T_x$) self-assembled microgel film by means of hydrogen bonding linkage. Benefiting from the rich hydroxyl groups on the MFC, the $Ti_3C_2T_x$ nanosheets coated on the MFC in a time scale of minutes (within 1 min) instead of hours. The ultralong 1D frame of MFC effectively mitigated the re-aggregation of $Ti_3C_2T_x$ nanosheet. The fluffy MFC@$Ti_3C_2T_x$ film structure and the constructed 1D/2D conducting $Ti_3C_2T_x$ pathways in horizontal and vertical directions endowed the fast ion transport of the electrolytes and the improved accessibility to the $Ti_3C_2T_x$ surface. As a result, the freestanding MFC@$Ti_3C_2T_x$ microgel film delivered a high specific capacitance of 451F/g. And the rate performance was increased to 71% from the 64% of that of pristine $Ti_3C_2T_x$ film. Furthermore, the tensile strength of MFC@$Ti_3C_2T_x$ film was also promoted to 46.3 MPa, 3 folds of that of the pristine $Ti_3C_2T_x$ film, due to the high strength of MFC and the hydrogen bonding effect.



Recently, 2D layered materials always gain tremendous attraction in the fields of electromagnetic interference shielding [1], catalysis [2], photothermal conversion [3] and energy storage field [4,5] for their unique characteristics, such as their planar geometry with atomic or molecular thickness [6,7], easy to process [8,9] and more exposed atom [10]. Among the existing 2D nanomaterials, the thriving family, MXene ($M_{n+1}X_nT_x$), as one of the most promising electrode materials, is standing out for their unique combination of metallic conductivity, nanosheet processability, hydrophilicity and widely tunable properties [11–13], where, M is an early transition metal such as Ti, X is C or N, and $T_x$ indicates the different functional groups (—O, —OH and —F) on the surface of metal layers. However, the self-aggregation of $Ti_3C_2T_x$ nanosheets due to the strong interlayer van der Waals interaction or hydrogen bonding deteriorates ionic dynamical diffusion, bringing about low accessibility of the electrolyte ions [14,15]. As a result, their performance in many fields is hindered severely by the aggregate phenomenon.

Hitherto, two approaches have been proposed for alleviating the self-stacking as well as enhancing ion transport kinetics, including construction of porous 3D structures [16,17] and introduction of interlayer pillars [18]. Nevertheless, the mechanical performance is rarely reported in above works, which is also crucial for practical supercapacitor application as a free-standing film. Actually, numerous efforts have been devoted to reinforce the mechanical strength of $Ti_3C_2T_x$ film, typically, introducing the nano-scale polymers (such as polyvinyl alcohol, bacteria cellulose and cellulose nanofiber) [19–21]. Unfortunately, the improvement of mechanical properties is at the expense of electrochemical performance. Generally, the capacitance of these nanocomposite films decreased quickly with the addition of nano-scale polymers due to the reduced interlayer conductivity. Thereby, there is much room in developing MXene-based materials to realize the trade-off between mechanical properties and electrochemical performance.

Herein, a novel strategy was proposed to fabricate anti-aggregation MFC@$Ti_3C_2T_x$ film electrode towards promoted electrochemical performance as well as mechanical strength. Cellulose with micron diameter (MFC) was selected as reinforcing materials due to their high aspect ratio, abundant of —OH groups and high Young's modulus (>150 GPa) [22]. In designed architecture, the $Ti_3C_2T_x$ nanosheets would be coating 1D MFC to produce MFC@$Ti_3C_2T_x$ microgel quickly owing to the rich —OH groups on MFC, hereby the 1D/2D conducting $Ti_3C_2T_x$ pathways in horizontal and vertical directions was constructed. As-prepared MFC@$Ti_3C_2T_x$ microgel not only suppresses the aggregation of $Ti_3C_2T_x$ nanosheets efficiently, but the mechanical properties of MFC@$Ti_3C_2T_x$

* Corresponding author.
*E-mail address:* yaozhongping@hit.edu.cn (Z. Yao).

https://doi.org/10.1016/j.cclet.2021.03.025

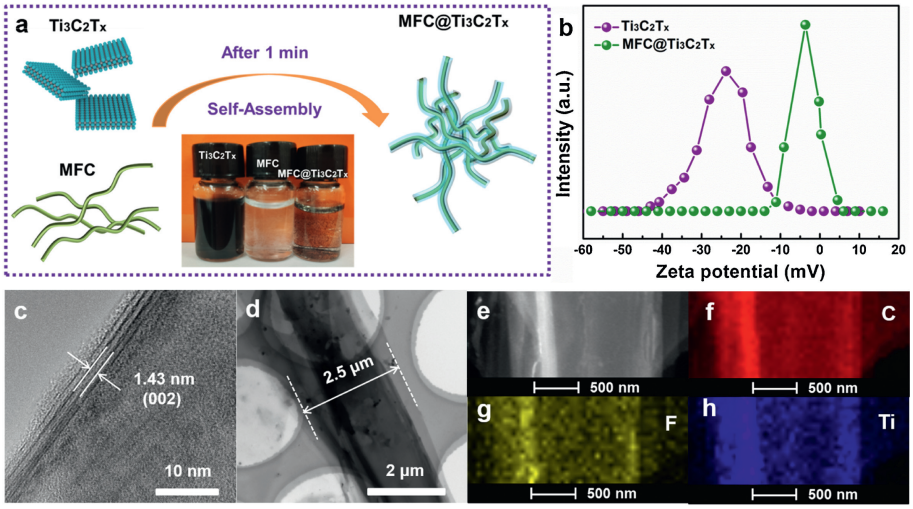


**Fig. 1.** (a) Schematic illustrating the fabrication process of MFC@$Ti_3C_2T_x$ microgel, the inset is digital photo of $Ti_3C_2T_x$ colloid solution (left), MFC solution (middle) and diluted MFC@$Ti_3C_2T_x$ microgel dispersions (right). (b) Zeta potentials of $Ti_3C_2T_x$ and MFC@$Ti_3C_2T_x$ dispersions. (c) HR-TEM image of $Ti_3C_2T_x$ nanosheets, (d) TEM image of MFC@$Ti_3C_2T_x$ dispersions. (e) STEM image of MFC@$Ti_3C_2T_x$ and the corresponding EDX elemental mapping of (f) C, (g) F and (h) Ti.

film have enhanced due to the framework of 1D MFC. As a result, the rate performance of MFC@$Ti_3C_2T_x$ film is increased from 64% to 71% profit by the unique anti-aggregation structure for fast ion transport. What is more, the self-assembled MFC@$Ti_3C_2T_x$ film could deliver an enhanced specific capacitance of 451 F/g at 1 A/g and superior tensile strength of 46.3 MPa, the balance of the energy storage and mechanical strength is realized in such anti-aggregation MFC@$Ti_3C_2T_x$ free-standing film.

The $Ti_3C_2T_x$ colloid solution was first prepared by etching $Ti_3AlC_2$ in HCl and LiF solution. After the introduction of MFC with abundant —OH groups (Fig. S2 in Supporting information) [23], the MFC@$Ti_3C_2T_x$ microgel was synthesized successfully within 1 min (Video S1 in Supporting information) due to the strong hydrogen bonding linkage between the terminations (*e.g.*, —F, —O and —OH) on the $Ti_3C_2T_x$ nanosheets and —OH groups on the MFC. Consequently, Because of the micron-sized average diameter of MFC (around 2 μm), the formed large-scale MFC@$Ti_3C_2T_x$ microgel greatly decreased the vacuum filtration time (filter membrane with 0.22 μm pore size), and the acquisition of MFC@$Ti_3C_2T_x$ film only took several minutes. Based on the huge size differences of $Ti_3C_2T_x$ nanosheets to MFC, $Ti_3C_2T_x$ nanosheets were self-assembled parallel to the radial direction of MFC. After coating, each 1D MFC@$Ti_3C_2T_x$ would interconnect each other to generate larger microgel, the schematic diagram of synthesis process of MFC@$Ti_3C_2T_x$ *via* self-assembly process is illustrated in Fig. 1a. The digital photos of the obtained MFC@$Ti_3C_2T_x$ film by vacuum-assist filtration in Fig. S3 (Supporting information) indicates much looser and coarser than that of the $Ti_3C_2T_x$ film, which means that the alleviation of stacking, accompanied by the improved dispersity of $Ti_3C_2T_x$ nanosheets, such anti-aggregation structure could be seen in Fig. S4d. As a result, more electrochemical active sites would be exposed for such anti-aggregation architecture of MFC@$Ti_3C_2T_x$ microgel. As for the MFC@$Ti_3C_2T_x$ free-standing films, distinct ultralong MFC could be observed in Fig. S4c (Supporting information), which is the guarantee for the robust mechanical strength. Fig. 1b shows the zeta potentials of $Ti_3C_2T_x$ and MFC@$Ti_3C_2T_x$ dispersions are −23 mV and −3 mV, respectively. The positive shift of the zeta potential demonstrates the negative potential on $Ti_3C_2T_x$ surface is partially offset by the strong hydrogen bonding linkage, further confirming the successful self-assembly process of the MFC@$Ti_3C_2T_x$ microgel.

Fig. S5 (Supporting information) shows the SEM images of $Ti_3C_2T_x$ nanosheet, MFC and MFC@$Ti_3C_2T_x$ microgel. Ultrathin 2D $Ti_3C_2T_x$ nanosheet is similar to the graphene, large-scaled cellulose is composed of much ultralong nanocellulose. Basis on the characteristic of MFC, MFC@$Ti_3C_2T_x$ microgel featuring 1D structure, the diameter and the length of are ~2.5 μm, ~120 μm, separately, with the high aspect ratio of 50. Fig. 1c is the TEM image of $Ti_3C_2T_x$ nanosheets, stacked 3 ~ 4 layers, which the thickness is about 3 nm (Fig. S6 in Supporting information). In addition, the interlayer spacing of $Ti_3C_2T_x$ is 1.43 nm,

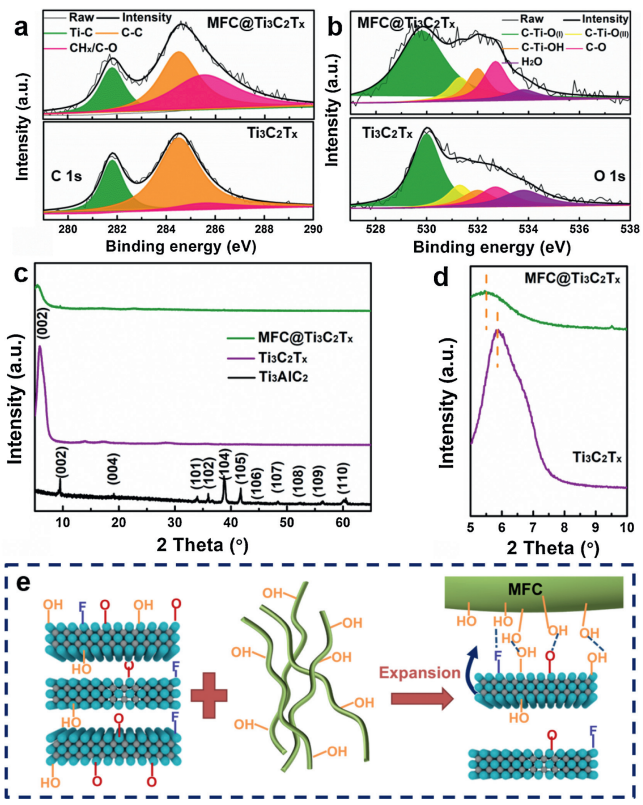


**Fig. 2.** (a) C 1s region and (b) O 1s region component peaks fitting of XPS spectra of $Ti_3C_2T_x$ and MFC@$Ti_3C_2T_x$ film. (c) XRD patterns of $Ti_3AlC_2$, $Ti_3C_2T_x$ and MFC@$Ti_3C_2T_x$. (d) Corresponding enlarged XRD patterns of $Ti_3C_2T_x$ and MFC@$Ti_3C_2T_x$. (e) Schematic illustrating the expansion of interlayer spacing in MFC@$Ti_3C_2T_x$.

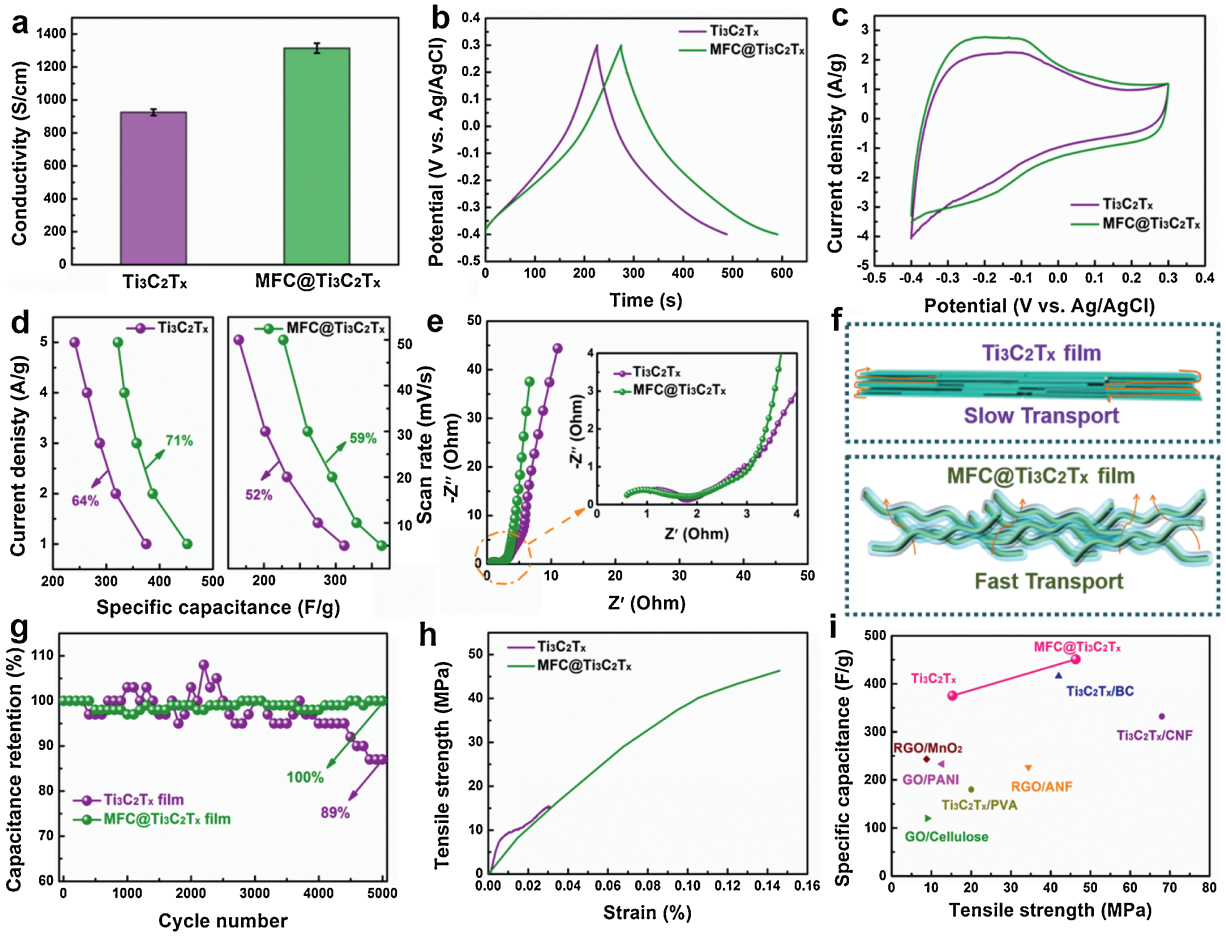


**Fig. 3.** (a) Conductivity of $Ti_3C_2T_x$ and MFC@$Ti_3C_2T_x$ films. (b) GCD curves at 1 A/g and (c) CV profiles at 5 mV/s for $Ti_3C_2T_x$ and MFC@$Ti_3C_2T_x$ electrodes. (d) Rate performance calculated from GCD and CV measurements. (e) EIS data of $Ti_3C_2T_x$ and MFC@$Ti_3C_2T_x$ electrodes. The inset shows the magnified high-frequency region. (f) Schematic illustration of ion transport channel of different films. (g) Cycling performance of $Ti_3C_2T_x$ and MFC@$Ti_3C_2T_x$ electrodes at 10 A/g. (h) Tensile stress–strain curves of $Ti_3C_2T_x$ and MFC@$Ti_3C_2T_x$ films. (i) Comparison of the capacitance versus mechanical strength of the MFC@$Ti_3C_2T_x$ film with some other notable reported composites in the literature.

corresponding to the (002) plane of $Ti_3C_2T_x$. Fig. 1d is the TEM image of MFC@$Ti_3C_2T_x$, as expected, distinct analogous core-shell architecture was formed. The thickness of MFC@$Ti_3C_2T_x$ is about 2.5 μm, in good agreement with that from SEM characterizations (Figs. S5c and d in Supporting information). Figs. 1e–h are the EDX elemental mapping results, which also show a clear interface between MFC and $Ti_3C_2T_x$, further indicating explicitly the formation of MFC@$Ti_3C_2T_x$ architecture.

The XPS spectra of $Ti_3C_2T_x$ and MFC@$Ti_3C_2T_x$ films in the C 1s region and O 1s region is shown in Figs. 2a and b. It could be seen that the contents of C-O/$CH_x$ increase significantly due to the introduction of organic MFC. In addition, the contents of T-C bonding have negligible change, which proves that connecting with MFC would not break the internal Ti-C bonding of $Ti_3C_2T_x$. This result demonstrates that the self-assembling strategy is not only facile but also nondestructive, and it could be further demonstrated in Ti 2p region (Fig. S7 in Supporting information). The XRD data of $Ti_3C_2T_x$ and MFC@$Ti_3C_2T_x$ is represented in Fig. 2c. The (104) main peak ($2\theta = 39°$) of precursor MAX is disappeared in composition of the $Ti_3C_2T_x$, suggesting that the Al element is successfully removed during the etching process. Additionally, the (002) peak is broadened and shift to 5.9° from 9.5°, manifesting that the c-lattice parameter and the interlayer spacing of $Ti_3C_2T_x$ is 30 Å and 15 Å, respectively. The value of interlayer spacing (15 Å) is closed to the results of TEM analysis (1.43 nm). After bonding with MFC, the (002) peak shift from 5.9° to 5.5° (Fig. 2d), revealing that the interlayer spacing is expanded from 15 Å to 15.9 Å. Considering that the large diameter of the MFC, it is impossible to intercalation the narrow interlayer of $Ti_3C_2T_x$ nanosheets (only 1.5 nm). Thus, the increasing interlayer spacing may be due to the pulling effect of hydrogen bonding. According to the results of TEM of MFC@$Ti_3C_2T_x$ microgel and Fig. 1a, single coated MFC@$Ti_3C_2T_x$ would connect each other, thereby the intermediate $Ti_3C_2T_x$ nanosheets would be pulled and expanded due to the stronger hydrogen linkage between MFC and $Ti_3C_2T_x$, as described in Fig. 2e. Such expanded interlayer spacing in favor of the intercalation of $H^+$ ion, and thus more faradic reaction could be occurred as follows:

$$Ti_3C_2(OH)_xO_yF_z + \delta H^+ + \delta e^- = Ti_3C_2(OH)_x + \delta O_{y-\delta}F_z \quad (1)$$

Different from the decreased conductivity arise from introduction of nano-scale polymers, the micro-scale MFC would not affect the charge transport of $Ti_3C_2T_x$ nanosheets. From Fig. 3a, strikingly, the conductivity MFC@$Ti_3C_2T_x$ film is enhanced compared to the encounter $Ti_3C_2T_x$ film. Ultralong 1D/2D conducting $Ti_3C_2T_x$ pathway is responsible for the promoted charge transport, however, as increasing the contents of MFC, the conductivity of composites film became decreased due to the excess insulator MFC, some exposed 1D MFC would block the electron transport in the planar dimension, thus the conductivity investigated by four-point probe technique would be decreased, as shown in Fig. S8 (Supporting information). The electrochemical performance of $Ti_3C_2T_x$ and MFC@$Ti_3C_2T_x$ electrode is carried out in three-electrode configuration. Fig. 3b shows the GCD curves of different films at 1 A/g, it could be observed that the discharge time of

MFC@$Ti_3C_2T_x$ electrode is longer than that of the pristine $Ti_3C_2T_x$ electrode, and the specific capacitance of $Ti_3C_2T_x$ electrode and MFC@$Ti_3C_2T_x$ electrode are 375 F/g and 451 F/g, respectively. The value of 451 F/g at 1 A/g in MFC@$Ti_3C_2T_x$ electrode is higher than most ever-reported anti-aggregated $Ti_3C_2T_x$-based electrode for supercapacitors (Table S1 in Supporting information). The enhanced capacitance in MFC@$Ti_3C_2T_x$ electrode is not only due to the increase of interlayer spacing, more the point, attributing to the shorten of ion diffusion channel [24,25]. Fig. 3c exhibits the CV curves of different films at 5 mV/s. The shape of the deviated from rectangle indicated the pseudocapacitance of the $Ti_3C_2T_x$ material, and the larger CV area in MFC@$Ti_3C_2T_x$ reveals the promoted charge storage. Based on specific capacitance from the GCD and CV curves at different current density and scan rate (Figs. S9 and S10, Table S2 in Supporting information), the rate performance is shown in Fig. 3d. It is not hard to find that the rate performance both increased by 7%, more importantly, the capacitance retained 71% after current density up to 5 A/g. Such enhanced rate performance is ascribing to the more accessible surface of $Ti_3C_2T_x$ nanosheet for electrolyte. Similar results could be found in EIS curves (Fig. 3e). After adding MFC, the high frequency region still maintained a negligible semicircle, proving excellent conductivity of MFC@$Ti_3C_2T_x$ electrode. Comparing the slope of the straight line in the low frequency region, it could be found that the MFC@$Ti_3C_2T_x$ electrode possessed higher slope, indicating that the diffusion impedance has reduced in MFC@$Ti_3C_2T_x$ electrode. Consequently, introduction of MFC could ease the stacking phenomenon between the layers as well as shortened the ion transport path greatly. Based on above result, compared with the compact $Ti_3C_2T_x$ film, looser MFC@$Ti_3C_2T_x$ microgel film provide the faster ion transport, as displayed in Fig. 3f. The cycling performance of pristine $Ti_3C_2T_x$ and MFC@$Ti_3C_2T_x$ electrodes at 10 A/g is shown in Fig. 3g. The MFC@$Ti_3C_2T_x$ electrode could keep initial capacitance after 5000 cycles, which better than that of pristine $Ti_3C_2T_x$ electrode, confirming its good cycle stability. Concluding the factor of improved electrochemical performance of MFC@$Ti_3C_2T_x$ electrode, the coated anti-aggregation structure is mainly account for larger interlayer spacing (hydrogen pulling effect), fast ion (looser architecture) and charge (1D/2D conducting pathway) transport. Considering the practical application in aqueous electrolyte, the mechanical properties of $Ti_3C_2T_x$-based film must be taken into account. Fig. 3h and Fig. S11 (Supporting information) are the tensile stress–strain curves of $Ti_3C_2T_x$ and MFC@$Ti_3C_2T_x$ films. The stress strength of MFC@$Ti_3C_2T_x$ film is up to 46.3 MPa owning to the synergistic bonding effect, leading to 3-fold improvement in competition of pristine $Ti_3C_2T_x$ film (16.1 MPa). Fig. S12 (Supporting information) is the photograph of a piece of 7 mm wide strip made from MFC@$Ti_3C_2T_x$ film, which can hold a 105 g weight, ~20,000 times its own weight. The plot of the gravimetric specific capacitance versus mechanical strength in Fig. 3i shows that the MFC@$Ti_3C_2T_x$ electrodes display the superior integration of the capacitance and mechanical strength among some of the previously reported notable supercapacitor electrodes, such as $Ti_3C_2T_x$/PVA [19], $Ti_3C_2T_x$/BC [20], $Ti_3C_2T_x$/CNF [21], RGO/ANF [26], GO/PANI [27], GO/cellulose [28] and RGO/$MnO_2$ [29], This indicates that in MFC@$Ti_3C_2T_x$ composites, an optimized trade-off between mechanical properties and energy storage is realized, where the mechanical strength is greatly improved compared to pristine $Ti_3C_2T_x$ film while the electrochemical properties of $Ti_3C_2T_x$ also improved.

In summary, the green and accessible 1D MFC was introduced into 2D $Ti_3C_2T_x$ nanosheets to fast fabricate anti-aggregation MFC@$Ti_3C_2T_x$ microgel. This facile and time-saving strategy to assembling 2D $Ti_3C_2T_x$ into a 1D/2D conducting channel is definitely nondestructive. Surprisingly, benefiting from the alleviation of self-stacking and shortened ion transport pathway of $Ti_3C_2T_x$ nanosheets, 71% rate performance was realized in aqueous electrolyte. Besides, the self-assembly MFC@$Ti_3C_2T_x$ microgel film exhibited an improved capacitance of 451F/g as well as the outstanding mechanical stress of 46.3 MPa, which is a guarantee for the practical potential. In addition, the cycling performance of MFC@$Ti_3C_2T_x$ electrode could withstand 5000 cycles without any capacitance decay. This fast self-assembly approach provides a new sight to construct anti-aggregation structure between 1D fibers and 2D nanosheets.

## Declaration of competing interest

The authors declare that they have no financial and personal relationships with other people or organizations that can inappropriately influence our work, there is no professional or other personal interest of any nature or kind in any product, service and/or company that could be construed as influencing the position presented in, or the review of, the manuscript entitled.

## Acknowledgments

This work was supported by National Natural Science Foundation of China (No. 51571076) and Open project of State Key Laboratory of Urban Water Resource and Environment of Harbin Institute of Technology (No. HCK202115).

## Appendix A. Supplementary data

Supplementary material related to this article can be found, in the online version, at doi:https://doi.org/10.1016/j.cclet.2021.03.025.

## References

[1] M. Cao, J. Shu, X. Wang, et al., Annalen. der. Physik. 531 (2019) 1800390.
[2] J.L. Gunjakar, T.W. Kim, H.N. Kim, I.Y. Kim, S.J. Hwang, J. Am. Chem. Soc. 133 (2012) 14998–15007.
[3] H. Lin, Y. Wang, S. Gao, Y. Chen, J. Shi, Adv. Mater. 20 (2017) 1703284.
[4] J. Liu, X. Liu, Adv. Mater. 24 (2012) 4097–4111.
[5] C. Long, X. Chen, L. Jiang, L. Zhi, Z. Fan, Nano Energy 12 (2015) 141–151.
[6] B. Sun, S. Lou, W. Zheng, et al., Nano Energy 78 (2020) 105366.
[7] P. Xu, L. Peng, C. Wu, Y. Xie, Chem. Soc. Rev. 45 (2014) 3303–3323.
[8] X. Zhao, P. Song, C. Wang, A.C. Riis-Jensen, K.P. Loh, Nature 581 (2020) 171–177.
[9] C. Schliehe, B.H. Juarez, M. Pelletier, et al., Science 329 (2010) 550–553.
[10] X. Kong, Q. Liu, C. Zhang, Z. Peng, Q. Chen, Chem. Soc. Rev. 46 (2017) 2127–2157.
[11] X. Xie, Z. Wu, N. Zhang, Chin. Chem. Lett. 31 (2020) 1014–1017.
[12] L. Ji, H. Zhang, H. Ren, et al., Adv. Mater. 29 (2017) 1702367.
[13] M. Ghidiu, M.R. Lukatskaya, M. Zhao, Y. Gogotsi, M.W. Barsoum, Nature 516 (2014) 78–81.
[14] L. Xiu, Z. Wang, M. Yu, X. Wu, J. Qiu, ACS Nano 12 (2018) 8017–8028.
[15] Z. Xiao, Z. Yang, Z. Li, P. Li, R. Wang, ACS Nano 13 (2019) 3403–3412.
[16] Y. Yue, N. Liu, W. Liu, et al., Nano Energy 50 (2018) 79–87.
[17] Z. Wu, T. Shang, Y. Deng, Y. Tao, Q. Yang, Adv. Sci. 7 (2020) 1903077.
[18] J. Luo, C. Wang, H. Wang, et al., Adv. Funct. Mater. 29 (2019) 1805946.
[19] L. Zheng, E.R. Chang, M. Zhao, et al., Proc. Natl. Acad. Sci. 111 (2014) 16676.
[20] Y. Wang, X. Wang, X. Li, Y. Bai, H. Xiao, Adv. Funct. Mater. 29 (2019) 1900326.
[21] W. Tian, V.M. Armin, S.R. Michael, et al., Adv. Mater. 31 (2019) 1902977.
[22] Y. Qiang, A. Patel, I.M. Zloczower, Cellulose 27 (2019) 1–14.
[23] J. Yeo, S. Hwang, Int. J. Adhes. Adhes. 78 (2017) 89–94.
[24] J. Li, X. Yuan, C. Lin, et al., Adv. Energy Mater. 7 (2017) 1602725.
[25] K. Le, M. Gao, W. Liu, J. Liu, Z. Guo, Electrochim. Acta 323 (2019) 134826.
[26] R.K. Se, H. John, T. Zhou, et al., ACS Nano 11 (2017) 6682.
[27] D. Wang, F. Li, J. Zhao, et al., ACS Nano 3 (2009) 1745.
[28] W. Zhe, S. Yang, D. Wang, et al., Adv. Energy Mater. 1 (2011) 917.
[29] S. Afriyanti, Y. Ce, W. Xu, S.L. Pooi, Adv. Mater. 25 (2013) 2809.